Angular energy distribution and temporal evolution of pulses emitted from low-Z neonlike $J=0-1$ x-ray lasers

Peixiang Lu,*,† Yuelin Li,* and Ernst E. Fill

Max-Planck-Institut für Quantenoptik, Hans-Kopfermann-Strasse 1, D-85748 Garching, Germany

(Received 25 March 1996)

We report a systematic investigation of the angular energy distribution and temporal evolution of pulses emitted from low-Z neonlike $J=0-1$ lasers by comparing prepulse-induced lasing in different materials (S, Cl, Ca, Ti, Ni, Cu, and Zn) and at different driving energies in the main pulse and the prepulse. It is found that with a main pulse energy of 350 ± 35 J and a prepulse energy of 50 ± 5 J, the laser peaks about 4 mrad off axis with a divergence of 4.5–7.5 mrad for the low-Z materials S, Cl, Ca, Ti, and Ni. Under the same conditions for Cu, Zn, and Ge the laser peaks about 6–7 mrad off axis with a divergence of 5–8.2 mrad. The lasing pulse durations range from 146 to 349 ps for $Z=30-16$ and peak at 237–413 ps before the peak of the L-band emission or the $J=2-1$ lasing line. The beam deflection and divergence, as well as the pulse duration are quite insensitive to the energies of the main pulse and the prepulse. However, a lower driving main pulse energy brings lasing close to the peak of the L-band emission. [S1050-2947(96)00311-3]

PACS number(s): 42.60.By, 32.30.Rj, 52.50.Jm, 32.70.−n

I. INTRODUCTION

Since the demonstration of collisionally pumped neonlike Se soft x-ray lasing in [1,2], considerable progress has been achieved in understanding the physics and enhancing the performance of neonlike x-ray lasers in laser-produced plasmas. Lasing in elements ranging from Si [3] to Ag [4] have been demonstrated in laboratories around the world, in which the neonlike argon laser has been demonstrated both in a capillary discharge [5] and a laser-irradiated gas puff plasma [6]. Saturation has also been demonstrated for a number of neonlike lasers [7–11].

In recent years the use of the prepulse technique [12,13] has gained widespread acceptance and opened the door for producing x-ray lasing in low-Z neonlike ions. It also has solved the mystery of the anomalously weak $J=0-1$ line that has plagued our understanding of collisional x-ray lasers. One distinctive feature of all these experiments is the observation of strong lasing dominated by the $3p\,^1S_0-3s\,^1P_1$ transition only when the prepulse was used. This transition is commonly referred to as the $J=0-1$ line. Simulations [14,15] suggest that the prepulse is helping to create a larger, more uniform plasma with smaller density gradients which enables the $J=0-1$ laser to propagate better along the gain region. It is also shown that beam refraction is the main factor for lack of lasing in low-Z elements without the application of a prepulse. Therefore knowledge of the beam refraction and temporal evolution of the neonlike $J=0-1$ lasers is essential for understanding the physics and optimizing the performance.

At Max-Planck-Institut für Quantenoptik (MPQ), lasing in neonlike ions down to silicon ($Z=14$) has been demon-

strated using the prepulse technique [3,6,14,16–25]. However, the angular profile and temporal evolution of these low-Z neonlike x-ray lasers have not yet been systematically investigated. To better understand the physics of the low-Z neonlike $J=0-1$ x-ray lasers, as well as the effect of the prepulse on their performance, a systematic investigation of the angular energy distribution and temporal evolution of the laser pulse was carried out. A variety of materials (S, Cl, Ca, Ti, Ni, Cu, and Zn) have been investigated using an energy of 350 ± 35 J in the main pulse with a 50 ± 5-J prepulse. For the neonlike Ti laser the influence of the intensities of the main pulse and the prepulse on the beam deflection, the beam divergence, and the temporal profile were also investigated.

II. EXPERIMENTAL SETUP

Experiments were conducted at the Max-Planck-Institut für Quantenoptik using the Asterix IV iodine laser facility [26]. The Asterix IV laser generates up to 600 J at 1.315 μm in a 450-ps pulse. The spurious prepulse was measured by means of a photomultiplier and was found to be below 10^{-6} of the main pulse energy. A specially designed cylindrical lens array [27] produced a line focus about 150 μm wide and 30 mm long.

To obtain a well-defined prepulse, a pair of mirrors was inserted into the beam path before and after the final steering mirror, as described in Ref. [16]. The prepulse delay was set to 5.23 ns for these experiments. To adjust the prepulse contrast we used calibrated neutral density filters to attenuate the prepulse without affecting the energy in the main beam. Typically 350 J of energy were used in the main pulse (the total energy was around 415 J) which results in 17 TW/cm^2 on target. The beam energy varied within a range of ±10% over the course of these experiments.

The targets consisted of flat slabs, all with the same length of 25 mm. For the sulfur targets, fine powder was glued onto a 25-mm-long glass substrate with an optical finish. The targets were positioned with a spatial accuracy of $\pm5\,\mu$m by an

────────

*Permanent address: Shanghai Institute of Optics and Fine Mechanics, Academia Sinica, P.O. Box 800-211, 201800 Shanghai, China.

†FAX: 0049-89-32905-200; Electronic address: pgl@ipp-garching.mpg.de

alignment telescope and oriented with an angular accuracy of ± 1 mrad by self-collimation of the target using a He-Ne laser.

Time-integrated, angular resolved and time-resolved spectra of the axial emission from the two ends of the plasma column were recorded. For the time-integrated, angularly resolved spectra a transmission grating spectrometer coupled to a thinned backside illuminated charge-coupled device (CCD) was used [28]. The spectrometer used a 5000-line/mm free-standing gold transmission grating with a 50-μm-wide slit and was aligned along the x-ray laser axis. A 1-μm-thick Al filter was used to attenuate the x-ray lasing output for Ti, Ni, Cu, Zn, and Ge. To obtain angularly resolved data, the 50-μm-wide slit of the grating oriented with its long axis perpendicular to the target surface was located 17.5 cm in front of the CCD, which was 74 cm from the center of the target chamber. This provided angular coverage of about 17 mrad from the target surface in the direction of the main hydrodynamic expansion. The total wavelength range covered by the CCD was about 10.4 nm and by moving it in the dispersion direction different wavelength ranges can be obtained.

For time-resolved spectra, a transmission grating spectrometer was coupled to an x-ray streak camera operated with a photocathode consisting of a 110-nm-thick Al foil overcoated with a layer of 110 nm of CsI [29]. The spectrometer used a 1000-line/mm free-standing gold transmission grating with a 50-μm-wide slit and was aligned along the x-ray laser axis. The 50-μm-wide slit of the grating oriented parallel to the target surface was located 24 cm in front of the streak camera slit, which was 96 cm from the center of the target chamber. By changing the position of the grating slit along the direction perpendicular to the target surface, the streak camera can intercept x-ray beams refracted at different angles from the target surface. The resolution achieved was typically 50 ps temporally and 1 nm spectrally. An optical CCD was used to read out the data from the streak camera.

III. RESULTS AND DISCUSSION

Quite generally in all of the investigated materials (S, Cl, Ca, Ti, Ni, Cu, and Zn) strong lasing on the $J=0-1$ line ($3p\,^1S_0 - 3s\,^1P_1$) was observed with a prepulse. The $J=0-1$ lasing wavelengths are 60.8, 52.9, 38.3, 32.6, 23.1, 22.1, and 21.2 nm for S, Cl, Ca, Ti, Ni, Cu, and Zn, respectively [30]. All $J=0-1$ lines dominate both in the angularly resolved and temporally resolved axial spectra. For Ni, Cu, and Zn, we also see the $J=2-1$ lasing lines. The necessity of a prepulse for the $J=0-1$ lasing line and the sensitivity of the laser output to the intensities of the main pulse and the prepulse can be found in several recent papers [3,14,16–25].

A. Angular distribution of neonlike $J=0-1$ lasers

Figures 1(a), 1(b), and 1(c) give typical images of the axial angularly resolved spectra showing the lasing lines obtained from 25-mm-long Si, Ti, and Zn targets and lineouts at the spectral center of the $J=0-1$ lasing lines. The intensity of an individual lasing line was obtained by subtracting the background continuum near the lasing line. The zero

angle corresponds to the axis of the target, defined by the alignment telescope. The obstruction of the beam at zero angle can be clearly seen in Fig. 1. The data show a narrow divergence and a certain deflection angle for all the neonlike $J=0-1$ lasing lines. From Fig. 1, one can see that S and Ti lasers have a smaller deflection angle of 4 mrad compared with the Zn laser (7 mrad). The S laser has a wider beam divergence of 7.5 mrad but a weaker lasing intensity compared with the Ti (5.2 mrad) and the Zn (5.6 mrad) lasers. For Ti and Zn lasers, a 1-μm-thick Al foil was used. Figure 2 displays the normalized angular energy profiles of the $J=0-1$ lasers from several materials. The angular profile of the Ge laser is also presented in Fig. 2 for comparison. One can clearly see that the S, Ti, and Ni lasers have a small deflection angle of ~ 4 mrad while Zn and Ge lasers have a larger deflection angle of 6–7 mrad. For Cl and Ca lasers using NaCl and CaF$_2$ targets, their deflection angles are similar to those of S, Ti, and Ni while their divergences are slightly smaller, about 4.5 mrad. For the Cu laser, the deflection angle is similar to that of Zn and its divergence is about 5.3 mrad.

We can see from Fig. 2 that the beam divergences [full width at half maximum (FWHM) of the angular profile] of all neonlike $J=0-1$ lasers are quite similar (4.5–5.6 mrad) except that S (7.5 mrad) and Ge (8.2 mrad) have larger beam divergences. For S, its large divergence is possible due to its lower gain coefficient of 1.5 cm^{-1} [3]. For Ge, we conclude that the lasing has a wider gain region compared with those of neonlike Ni, Cu, and Zn $J=0-1$ lasers because the laser in Ni, Cu, Zn, and Ge has a similar gain coefficient of about 4 cm^{-1} [22].

The measured deflection angles do not depend strongly on the material for the large range of nuclear charges from $Z=16$ (sulfur) to $Z=32$ (germanium). Apparently this is caused by two effects which partially compensate each other: For a low nuclear charge the longer wavelength leads to a larger deviation of the refraction index from unity and thus to a stronger deflection away from the target. On the other hand, for higher nuclear charges lasing occurs at a higher electron density for which the electron density gradient should be larger.

The interplay between these two effects can be assessed semiquantitatively by means of simple theory: Let the electron density distribution at time of lasing in a direction x away from the target be given by a Gaussian function,

$$N_e = N_{e,0} \exp(-x^2/x_0^2), \qquad (1)$$

as can be derived from a self-similar solution of the hydrodynamic equation if a spatially isothermal plasma expands adiabatically [31]. The spatial extension of the plasma eventually increases linearly with time, $x_0 \sim C_s t_p$, where for t_p the time between the prepulse and main pulse can be set and the ion sound velocity $C_s = (qT_e/A)^{1/2}$, where q is the ionic charge, T_e the electron temperature, and A the atomic weight of the material. A is approximated by $2Zm_p$, where m_p is the mass of the proton. Here $T_e \propto I_{\text{prepulse}}^{2/3}$ under a steady-state assumption [32]. If the preplasma is dominated by Ne-like ions, then $C_s = [(Z-10)T_e/2Zm_p]^{1/2}$.

Lasing occurs around an optimum electron density which, according to Elton's scaling [33], is given by
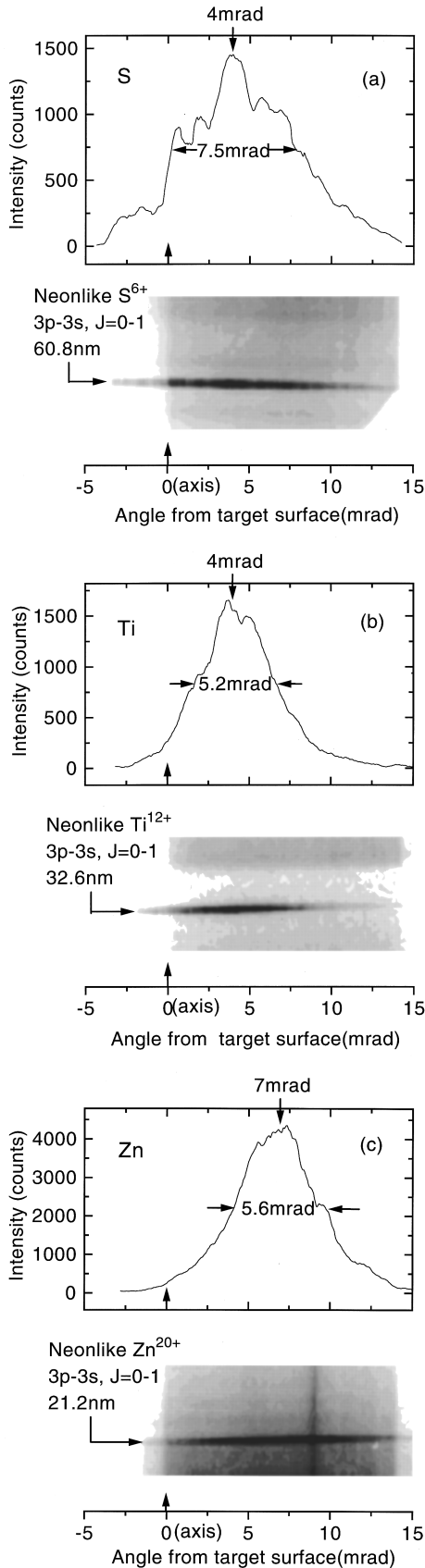
FIG. 1. On-axis time-integrated but angularly resolved images of the neonlike (a) S, (b) Ti, and (c) Zn spectra showing $J=0-1$ lasers obtained from a 25-mm-long target illuminated at an intensity of 17 TW/cm^2 with a 2.5-TW/cm^2 prepulse, and lineouts at the spectral center of the laser lines. A 1.0-μm-thick aluminum filter was used to attenuate the Ti and Zn spectra.
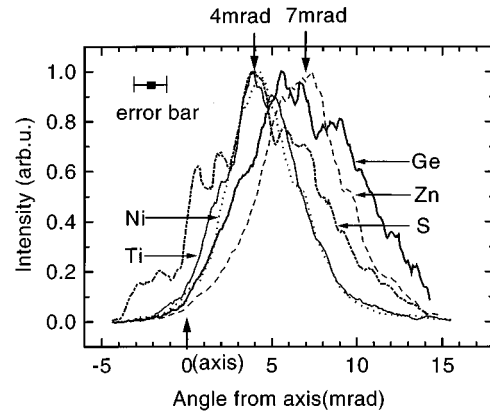

FIG. 2. Normalized angular energy profiles of the neonlike S, Ti, Ni, Zn, and Ge $J=0-1$ lasers obtained from a 25-mm-long target illuminated at an intensity of 17 TW/cm^2 with a 2.5-TW/cm^2 prepulse.

$N_{e,\mathrm{opt}}=4\times10^{15}(Z-9)^{3.75}$ cm^{-3}. If the density distribution is sufficiently smooth, we can calculate the deflection angle approximately by using the local density gradient at $N_e=N_{e,\mathrm{opt}}$, given by

$$dN_e/dx=(2N_{e,\mathrm{opt}}/x_0)[\ln(N_{e,0}/N_{e,\mathrm{opt}})]^{1/2}. \qquad (2)$$

In a plasma the deflection angle of a ray which is initially parallel to the target surface becomes, after propagating a distance L through a medium with a constant electron gradient,

$$\Phi=(L/4N_{\mathrm{cr}})(-dN_e/dx), \qquad (3)$$

where N_{cr} is the critical electron density for the x ray. Inserting (2) into (3) we obtain for the far-field deflection angle the simple expression

$$\Phi=(L/2x_0)(N_{e,\mathrm{opt}}/N_{\mathrm{cr}})[\ln(N_{e,0}/N_{e,\mathrm{opt}})]^{1/2}. \qquad (4)$$

Equation (4) shows the dependence of the deflection angle on the electron density of the x-ray laser. The wavelength dependence enters through the critical density, which is given by $N_{\mathrm{cr}}=1.1\times10^{27}\lambda^{-2}$ cm^{-3}, with λ in nm.

Using Elton's scaling for the wavelength of neonlike $J=0-1$ lasers, viz., $\lambda=460/(Z-9)$ nm, and taking both T_e and $N_{e,0}$ as independent of Z, we see that the deflection angle depends on the nuclear charge as

$$\Phi=1.8\times10^{-1}[2Z/T_e(Z-10)]^{1/2}(Z-9)^{1.75}$$
$$\times\{\ln[N_{e,0}/4\times10^{15}(Z-9)^{3.75}]\}^{1/2}\ \mathrm{mrad}. \qquad (5)$$

Equation (5) shows that Φ is only weakly dependent on both T_e and $N_{e,0}$. Figure 3 gives the calculated deflection angles of neonlike $J=0-1$ x-ray lasers with different nuclear charge for $T_e=100$ eV and $N_{e,0}=N_c=6.45\times10^{20}$ cm^{-3}, where the N_c is the critical density of the iodine laser. Also presented in the figure are the measured angles at peak and half maximum of the lasing angular profiles. One can see from Fig. 3 that the calculated deflection angle is weakly dependent on nuclear charge, which is consistent with our experimental result that the measured deflection angles do
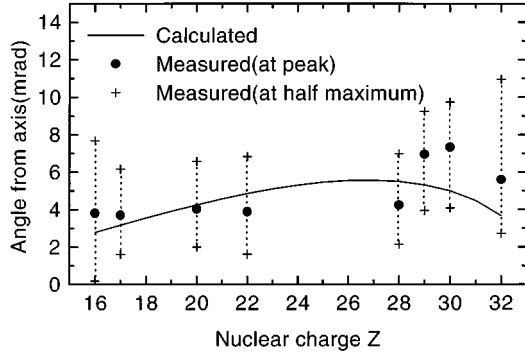
FIG. 3. Calculated deflection angles of neonlike $J=0-1$ x-ray lasers vs nuclear charge Z for a target length of 25 mm, Te$=100$ eV, and $N_{e,0}=N_c=6.45\times10^{20}$ cm^{-3}, where the N_c is the critical density of iodine laser. Also presented are the measured angles at peak (solid circle) and half maximum (cross) of the lasing angular profiles.

not vary strongly for the range of materials investigated. The larger measured deflection angles for Cu, Zn, and Ge lasers compared to those calculated can be attributed to the fact that these lasers lase close to the critical density of the iodine laser (6.45×10^{20} cm^{-3}) where the electron density profile may be steeper than the one obtained from the self-similar solution (a Gaussian function).

We also investigate the angular profile dependence on the intensities of the main pulse and the prepulse using the 32.6-nm laser in Ti. The x-ray lasing beam deflection angle and divergence (FWHM) are found to be not sensitive to the variation of the main pulse and the prepulse.

B. Temporal evolution of neonlike $J=0-1$ lasers

In these experiments, the slit of the grating of the streaked spectrometer was located at the angular maximum observed by the angularly resolved spectrometer to intercept the maximum of the lasing angular profile. The temporal evolutions of the $J=0-1$ lasing lines in S, Cl, Ca, Ti, Ni, Cu, and Zn were investigated. All data show that the neonlike $J=0-1$ x-ray lasing pulse is shorter than the pump laser pulse and occurs during the rising part of the pump laser pulse.

As examples, Figs. 4(a) and 4(b) give the streaked images of the neonlike S and Ti $J=0-1$ lasers recorded by the CCD readout with a (345 and 362 J) main pulse and a (48.7 and 51.1 J) prepulse, respectively. From Fig. 4, one can clearly see that lasing signals, as well as the zeroth-order and the L-band emission at a wavelength of about 2 nm. Because the photocathode of the streak camera has a 110-nm-thick Al substrate at the source side which behaves like a filter, all streak images have a low background and besides the lasing signals one can only see the zeroth order and the emission from the L band at a wavelength around 2 nm. Note that the high relative intensity of the L-band emission is due to the much higher sensitivity of the steak camera at short wavelengths. For Cu and Zn, the zeroth-order and the L-band emission are outside the range of the CCD camera and cannot be observed because the grating was moved far away from the target axis due to the large beam deflection. From Fig. 4(b), we can also see the second order of the Ti laser.
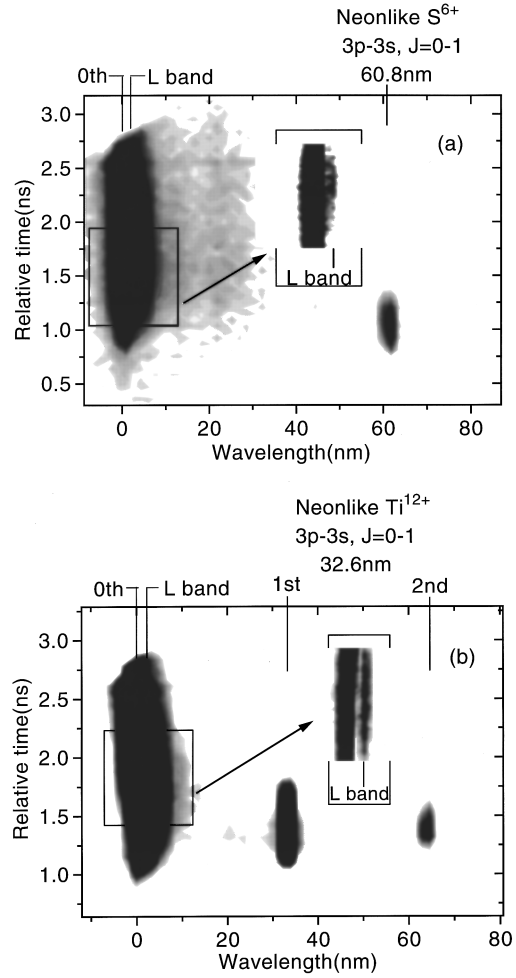

FIG. 4. On-axis streaked images obtained from the 25-mm-long (a) S and (b) Ti targets illuminated at an intensity of 17 TW/cm^2 with a 2.5-TW/cm^2 prepulse.

The wavelength scale is slightly nonlinear due to the distortion of the imaging intensifier of the streak camera. The first order of the Ti laser is seriously broadened along the temporal axis as well as the spectral axis due to saturation of the spectrometer. Similar phenomena are also observed for Ni, Cu, and Zn lasers and in this case we used the second order of the spectrum instead of the first order for analysis.

Figures 5(a) and 5(b) display the time histories of the $J=0-1$ lasing in neonlike S and Ni ions, and that of the L-band emission at wavelengths of about 2–3 nm, respectively. The temporal profiles of two neonlike $J=2-1$ Ni lasing lines at a wavelength of ~30 nm (29.8 and 30.4 nm, respectively), which are not resolved, are also seen in Fig. 5(b). From the figures, we can see that the peak of the $J=0-1$ lasing always appears several hundred ps (413 ps for S and 340 ps for Ni, respectively) in advance of the peak of the L-band emission, which is regarded as an approximate reference of the peak of the main driving pulse. It is also shown in Fig. 5(b) that the peak of $J=2-1$ lines appears 50 ps before the peak of the L band and 290 ps after the peak of the $J=0-1$ line. In comparison with the $J=0-1$ line of which the pulse duration is 256 ps, the pulse duration (FWHM) of the $J=2-1$ lines is considerably longer, about 346 ps. The temporal histories of the $J=0-1$ and 2–1 laser
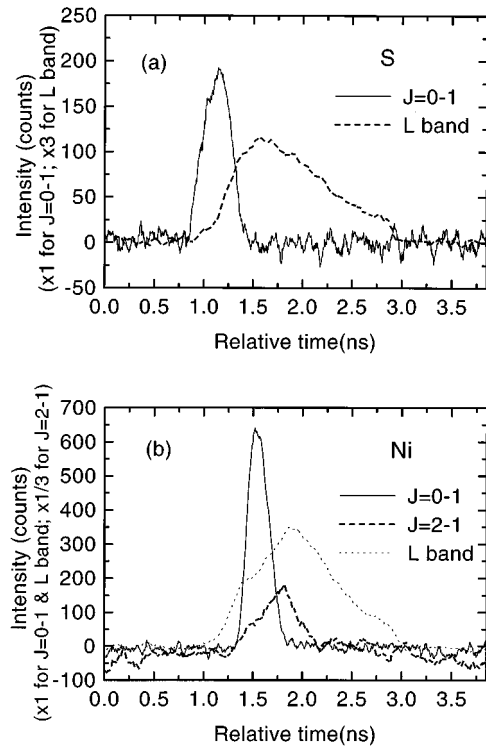
FIG. 5. Temporal lineout of the neonlike $J=0-1$ lasing lines obtained from the 25-mm-long (a) S and (b) Ni targets illuminated at an intensity of 17 TW/cm^2 with a 2.5-TW/cm^2 prepulse, corresponding to the spectral center of the laser lines. The temporal lineout of the L-band emission is also shown for reference.
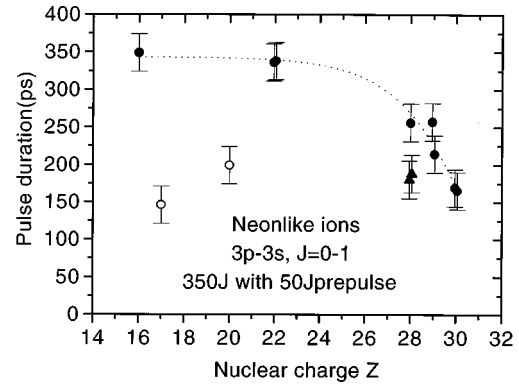

FIG. 6. The pulse duration (FWHM) of the neonlike $J=0-1$ laser vs the nuclear charge Z of the lasing gain material. The lasing targets were 25 mm long and were illuminated at an intensity of 17 TW/cm^2 with a 2.5-TW/cm^2 prepulse. The circle represents the data obtained from the peak intensity of the lasing angular profiles whereas the solid up triangle for Ni represents the data obtained from at an angle of 6.5 mrad, i.e., 2.5 mrad larger than the peak intensity angle. The open circles present the data obtained using compound targets. The data points of the Ni (two up triangles) and Zn (two solid circles) lasers are derived form the second- and the third-order spectrum, respectively.

lines in neonlike Cu and Zn ions were observed to be similar. Their pulse durations are 40–55 % of the driving pulse duration for the $J=0-1$ and 70–95 % for the $J=2-1$ lines, respectively.

The different time histories of the $J=0-1$ and $2-1$ lasing lines illustrate that the lasers occur in different plasma regions and that they are pumped by different pumping processes. The $J=0-1$ laser is predominantly pumped by direct monopole excitation from the neonlike ground state while other pumping processes, such as dielectronic recombination from F-like ions and cascading from higher levels, play a significant role on the $J=2-1$ lasers besides the direct monopole excitation from the neonlike ground state. In this case, pumping of the $J=0-1$ laser relies more on a high density and a high abundance of the ground state than that of $J=2-1$ lasers. As the plasma is stripped rapidly through the neonlike stage in this high density region, the conditions for gain production on the $J=0-1$ are quickly lost during the main pulse, and lasing can only occur early in time and is transient. The $J=2-1$ lasers have a longer pulse duration and peak later in time because they occur in a lower electron density region in which the neonlike ion abundance is maintained for a longer time due to the lower ionization rate.

The pulse duration (FWHM) of the neonlike $J=0-1$ laser as a function of nuclear charge Z is presented in Fig. 6. The circles represent data obtained from the peak intensity of the lasing angular profiles whereas the two solid up triangles for Ni represent the durations derived from the second and the third order of the neonlike Ni $J=0-1$ laser obtained at an angle of 6.5 mrad, i.e., 2.5 mrad larger than the peak inten-

sity angle. The two data points of the Zn lasers are also derived from the second- and the third-order spectrum, respectively. We use open circles to indicate the data obtained using compound targets, i.e., NaCl for Cl and CaF$_2$ for Ca, respectively. The error bars given in the figure are derived from a consideration of the measurement accuracy of ± 4–5 CCD pixels and the error from the time scaling of the streak camera. All shots were with a 350 ± 35-J main pulse and a 50 ± 5-J prepulse. The similar pulse durations (180 and 188 ps for Ni, 169 and 165 ps for Zn) derived from the second and third order of the spectra confirmed that the data derived from the second order instead of first order (when the laser was saturated) are correct. The temporal evolution of the Ni lasing obtained from 2.5 mrad off the angular peak is quite similar to that obtained from the peak, and only the pulse duration is 70 ps shorter. It was shown in Fig. 6 that the pulse duration of the neonlike $J=0-1$ lines increases with the decreasing nuclear charge Z except for Cl and Ca lasers for which compound targets were used.

Figure 7 shows the time of the neonlike $J=0-1$ lasing peak relative to the peak of L-band emission (open circles and up triangles) or of the $J=2-1$ lasing lines (solid circles) vs the nuclear charge Z. The data in Fig. 7 using circles were obtained with a main driving pulse energy of 350 ± 35 J with a prepulse of 50 ± 5 J. The data show that the time between the neonlike $J=0-1$ lasing peak and the peak of L-band emission or the $J=2-1$ lasing line increases slightly with decreasing nuclear charge Z. Data points for Ti for a smaller driving main pulse of a 100-J energy with 5- or 0.5-J prepulse are also shown in the figure (open up triangles). It is seen that for the small energy the time between the neonlike Ti $J=0-1$ lasing peak and the peak of L-band emission is much smaller compared to the one with standard energy of 350 ± 35 J. However, the delays at the 100-J main pulse are insensitive to the level of the prepulse (184 ps for 5-J prepulse and 186 ps for 0.5-J prepulse). Figures 8(a) and 8(b)
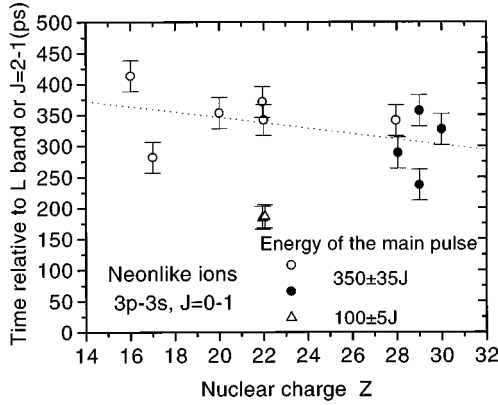
FIG. 7. The peak time of the neonlike $J=0-1$ laser relative to the peak of L-band emission or $J=2-1$ line vs the nuclear charge Z of the lasing gain material. The lasing target was 25 mm long. The open and solid circles represent the time relative to the peak of the L-band emission and to the $J=2-1$ lasing lines, respectively, obtained with a main pulse energy of 350 ± 35 J and a prepulse energy of 50 ± 5 J, respectively. The two open up triangles represent the time relative to the peak of the L-band emission obtained with a same main pulse energy of 100 ± 5 J and different prepulse energies of 5 and 0.5 J, respectively.

present the time histories of the Ti lasers obtained with the same prepulse of 5 J and two different main pulse energies of 380 and 100 J, respectively [the data in Fig. 8(b) were obtained from the first-order spectrum because the laser is too weak in the second order and the first order is not saturated for a 100-J main pulse]. For 100 J the pulse duration is
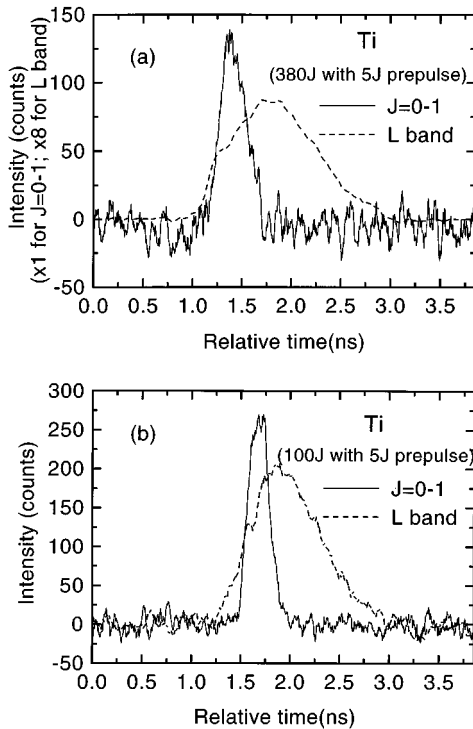

FIG. 8. Temporal lineout of the neonlike Ti $J=0-1$ lasing line (32.6 nm) from a 25-mm-long target with a prepulse energy of 5 J, corresponding to the spectral center. The main pulse energies are (a) 380 and (b) 100 J, respectively. The temporal lineout of the L-band emission is also shown for reference.
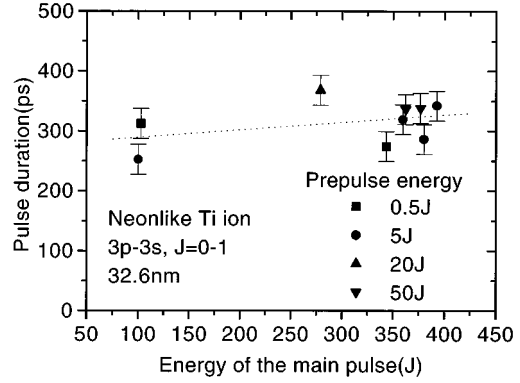

FIG. 9. The pulse duration (FWHM) of the neonlike Ti $J=0-1$ laser vs the energy of the main driving pulse with different prepulses. The target length is 25 mm.

slightly shorter (252 vs 286 ps at 380 J). A considerable difference is seen for the peak time relative to the L-band emissions (371 ps for 380 J and 184 ps for 100 J, respectively), implying that the starting time of the lasing is determined by the time at which the main pulse sufficiently heats the plasma.

We also varied the energy of the prepulse to investigate the pulse duration dependence on prepulse energy using the 32.6-nm laser in Ti. Figure 9 shows the pulse duration of the Ti laser as a function of the energy of the main driving pulse with different prepulses. As mentioned above, the pulse duration decreases slightly with decreasing main pulse energy, ranging from 252 to 368 ps. However, the duration of the lasing pulse was found to be insensitive to the prepulse level.

As mentioned above, the $J=0-1$ laser is dominantly pumped by direct monopole excitation from the neonlike ground state. The monopole excitation can be effective only at a high enough electron temperature, which is proportional to the excitation energy of the upper laser level relative to the ground state. This excitation energy ΔE_{2p-3p} scales as $\sim(Z-6.4)^{1.97}$ for low-Z materials [25]. We define a temperature of $\sim\Delta E_{2p-3p}/2$ as the threshold electron temperature for the neonlike $J=0-1$ lasing. Because of the lower-Z lasers have a lower threshold temperature due to their smaller excitation energy of the upper lasing level, during the period of the same main pulse, the electron temperature reaches the threshold earlier for lower-Z materials such as S and Ti than for Ni, Cu, and Zn, and therefore lasing occurs earlier. However, the electron temperature increases further during the main pulse, the plasma is rapidly overionized, and therefore the laser terminates before the peak of the main pulse. The longer pulse duration for lower-Z neonlike $J=0-1$ lasers such as S and Ti is understood by the fact that lasers in these materials appear in a region with a lower electron density. For the neonlike $J=0-1$ laser, the optimal electron density has a scaling with Z as $N_{opt}\sim(Z-9)^{3.75}$ [33]. The ionizing rate from neonlike to F-like ions depends linearly on the electron density and is relatively insensitive to the electron temperature. Therefore, when the main driving pulse arrives and heats the preplasma, the neonlike ions for the lower-Z materials such as S and Ti are ionized relatively slowly to F-like ions because of the lower electron density, maintaining an abundance of neonlike ions for a longer time. As a consequence the laser has a longer pulse duration. We
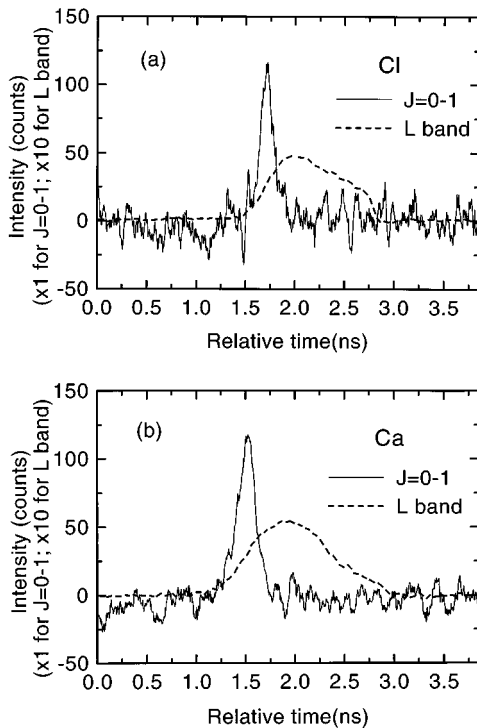
FIG. 10. Temporal lineout of the neonlike lasing lines from the 25-mm-long (a) NaCl and (b) CaF$_2$ targets illuminated at an intensity of 17 TW/cm^2 with a 2.5-TW/cm^2 prepulse, corresponding to the spectral center of the lasing lines. The temporal lineout of the L-band emission is also shown for reference.

should also point out that we are measuring the intensity, which has a different temporal profile than the gain. Due to the nonlinear relationship between the intensity and the gain, a higher peak gain will lead to a narrow duration in intensity even if the gain duration is similar. Thus the shorter pulse duration of higher-Z lasers may be a consequence of their higher gain. Finally, for a lower pumping energy, because the electron temperature reaches its threshold value at a much later time, the laser appears much closer to the peak of main pulse.

The reason for the abnormally short pulse durations observed for Cl (146 ps) and Ca (199 ps) as shown in Figs. 10(a) and 10(b) is not clear at the moment. We note that the targets for these two materials were compounds (NaCl in the case of Cl and CaF$_2$ in the case of Ca) whereas the targets of all other materials were made of pure element. It may be argued that the conditions in a compound target are less favorable for lasing since at the optimum electron density the number density of lasing ions is reduced. Indeed, in previous work [20,34] it was found that the gain coefficient for Cl, for

which a KCl target was used, was significantly lower (2.5 cm^{-1}) than for the other materials. However, in Ca, using a CaF$_2$ target, the gain (3.8 cm^{-1}) was similar to the gains of pure materials adjacent in nuclear charge. Thus the argument that a compound target is less favorable for lasing may only partially explain our experimental observation.

Another possible explanation rests on the fact that both target materials are transparent for the iodine laser driver radiation at 1.3 μm and thus the prepulse ablates less of the material, resulting in a smaller preplasma. However, the prepulse intensity used in our experiment was about 3×10^{12} W/cm^2, which is more than two orders of magnitude above the threshold intensity for optical damage. Therefore it is hard to conceive that there should be any difference in the generation of the preplasma.

IV. CONCLUSIONS

We have presented a systematic experimental investigation of angular energy distribution and temporal evolution of the low-Z neonlike $J=0-1$ x-ray lasers. The angular energy profiles show that all the neonlike $J=0-1$ lasing lines have a narrow beam divergence (the FWHMs are 4.5–8.2 mrad). The beam deflection angle is about 4 mrad for S, Cl, Ca, Ti, and Ni and 6–7 mrad for Cu, Zn, and Ge. The beam deflection and divergence are insensitive to the level of the main pulse and the prepulse. The time histories show that all neonlike $J=0-1$ lasers peak at the rising part of the driving main pulse and 237–413 ps before the peak of L-band emission or $J=2-1$ laser lines. With decreasing nuclear charge Z, the neonlike $J=0-1$ lasing peaks earlier and its pulse duration increases. The beam deflection and divergence, as well as the pulse duration do not change significantly when the main pulse and the prepulse energies were changed. However, when a low driving main pulse energy of 100 J was used the Ti lasing peaks much closer to the peak of the L-band emission.

[1] M. D. Rosen, P. L. Hagelstein, D. L. Matthews, E. M. Campell, A. U. Hazi, B. L. Whitten, B. J. MacGowan, R. E. Turner, and R. W. Lee, Phys. Rev. Lett. **54**, 106 (1985).

[2] D. L. Matthews, P. L. Hagelstein, M. D. Rosen, M. J. Eckart, N. M. Ceglio, A. U. Hazi, H. Medecki, B. J. MacGowan, J. E. Trebes, B. L. Whitten, E. M. Campell, C. W. Hatcher, A. M.

Hawryluk, R. L. Kauffman, L. D. Pleasance, G. Rambach, J. H. Scofield, G. Stone, and T. A. Weaver, Phys. Rev. Lett. **54**, 110 (1985).

[3] Y. Li, P. Lu, G. Pretzler, and E. E. Fill, Opt. Commun. (to be published).

[4] D. J. Fields, R. S. Walling, G. M. Shimkaveg, B. J.

MacGowan, L. B. Da Silva, J. H. Scofield, A. L. Osterheld, T. W. Phillips, M. D. Rosen, D. L. Matthews, W. H. Goldstein, and R. E. Steward, Phys. Rev. A **46**, 1606 (1992).

[5] J. J. Rocca, V. Shlyapstev, F. Tomasel, O. D. Cortazar, D. Hartshorn, and J. L. A. Chilla, Phys. Rev. Lett. **73**, 2192 (1994).

[6] H. Fiedorowicz, A. Bartnik, Y. Li, P. Lu, and E. E. Fill, Phys. Rev. Lett. **76**, 415 (1996).

[7] A. Carillon, H. Z. Chen, P. Dhez, L. Dwivedi, J. Jacoby, P. Jaegle, G. Jamelot, J. Zhang, M. H. Key, A. Kidd, A. Klisnick, R. Kodama, J. Krishan, C. L. S. Lewis, D. Neely, P. Norreys, D. M. O'Neil, G. J. Pert, S. A. Ramsden, J. P. Raucort, G. J. Tallents, and J. Uhomoibhi, Phys. Rev. Lett. **68**, 2917 (1992).

[8] S. Wang, Y. Gu, G. Zhou, S. Yu, S. Fu, Y. Ni, J. Wu, Z. Zhou, G. Han, Z. Tao, Z. Lin, S. Wang, W. Chen, D. Fan, G. Zhang, J. Sheng, H. Peng, T. Zhang, and Y. Shao, J. Opt. Soc. Am. B **9**, 360 (1992).

[9] J. A. Koch, B. J. MacGowan, L. B. Da Silva, D. L. Matthews, T. H. Underwood, P. J. Batson, and S. Mrowka, Phys. Rev. Lett. **68**, 3291 (1992).

[10] L. B. Da Silva, B. J. MacGowan, S. Mrowka, J. A. Koch, R. A. London, D. L. Matthews, and J. H. Underwood, Opt. Lett. **18**, 1174 (1993).

[11] P. Jaeglé, A. Carillon, P. Dhez, P. Goedtkindt, G. Jamelot, A. Klisnick, B. Rus, Ph. Zeitoun, S. Jacquemot, D. Mazataud, A Mens, and J. P. Chaurineau, in *X-ray Lasers 1994*, edited by D. C. Eder and D. L. Matthews (AIP, New York, 1994), p. 25.

[12] J. Nilsen, B. J. MacGowan, L. B. Da Silva, and J. C. Moreno, Phys. Rev. A **48**, 4682 (1993).

[13] J. Nielsen, J. C. Moreno, B. J. MacGowan, and J. A. Koch, Appl. Phys. B **57**, 309 (1993).

[14] Y. Li, G. Pretzler, E. E. Fill, and J. Nilsen, J. Opt. Soc. Am B **13**, 742 (1996).

[15] J. Zhang, S. T. Chunyu, Y. L. You, Q. R. Zhang, S. J. Yang, W. Z. Huang, D. Y. Wu, X. Q. Zhuang, S. P. Liu, Y. Q. Cai, F. Y. Du, X. D. Yuan, X. F. Wei, T. K. Zhao, H. S. Peng, and J. Nilsen, Phys. Rev. A **53**, 3640 (1996).

[16] E. E. Fill, Y. Li, D. Schlögl, J. Steingruber, and J. Nilsen, Opt. Lett. **20**, 374 (1995).

[17] E. E. Fill, Y. Li, and G. Pretzler, J. Sel. Topics Quantum Electron. **1**, 958 (1995).

[18] E. E. Fill, Y. Li, G. Pretzler, D. Schlögl, J. Steingruber, and J. Nilsen, Phys. Scr. **52**, 158 (1995).

[19] Y. Li, G. Pretzler, and E. E. Fill, Opt. Lett. **20**, 1026 (1995).

[20] Y. Li, G. Pretzler, and E. E. Fill, Phys. Rev. A **52**, R3433 (1995).

[21] Y. Li, G. Pretzler, E. E. Fill, and J. Nilsen, Appl. Phys. B **63**, 125 (1996).

[22] Y. Li, G. Pretzler, and E. E. Fill, Phys. Rev. A **51**, R4341 (1995).

[23] Y. Li, G. Pretzler, and E. E. Fill, Opt. Commun. **119**, 557 (1995).

[24] Joseph Nilsen, Yuelin Li, Peixiang Lu, Juan C. Moreno, and Ernst E. Fill, Opt. Commun. **124**, 287 (1996).

[25] Y. Li, G. Pretzler, P. Lu, and E. Fill (unpublished).

[26] H. Baumhacker, G. Brederlow, E. Fill, R. Volk, S. Witkowski, and K. J. Witte, Appl. Phys. B **61**, 325 (1995).

[27] W. Chen, S. Wang, C. Mao, B. Chen, and A. Xu, in *1990 Conference on Lasers and Electro-Optics*, Technical Digest Series Vol. 7 (Optical Society of America, Washington, DC, 1990), pp. 282 and 283.

[28] Y. Li, G. D. Tsakiris, and R. Sigel, Rev. Sci. Instrum. **66**, 80 (1995).

[29] G. D. Tsakiris, Proc. SPIE **1032**, 910 (1989).

[30] J. Nilsen and J. N. Scofield, Phys. Scr. **49**, 588 (1994).

[31] R. A. London and M. Rosen, Phys. Fluids **29**, 3813 (1986).

[32] See, for example, C. E. Max, in *Laser-Plasma Interaction*, edited by R. Balian and J. C. Adam (North-Holland, Amsterdam, 1982), p. 306.

[33] R. C. Elton, *X-Ray Lasers* (Academic, San Diego, 1990), p. 107.

[34] E. E. Fill, Yuelin Li, G. Pretzler, D. Schlögl, J. Steingruber, and J. Nilsen, Proc. SPIE **2520**, 134 (1995).